Proton dynamics in supercooled water by molecular dynamics simulations and quasielastic neutron scattering

Daniela Di Cola and Antonio Deriu
INFM-Dipartimento di Fisica, Università di Parma, Viale delle Scienze, I-43100 Parma, Italy

Marco Sampoli
INFM-Dipartimento di Energetica, Università di Firenze, Via Santa Marta 3, I-50139 Firenze, Italy

Alessandro Torcini[a)]
Theoretische Physik, Bergische Universität Gesamthochschule, Wuppertal, D-42097 Wuppertal, Germany

(Received 22 May 1995; accepted 22 November 1995)

A detailed study of the single-particle dynamics of liquid water in normal and supercooled regime has been carried out by comparing molecular dynamics (MD) simulation results with now available high resolution quasielastic neutron scattering (QENS) data. Simulation runs have been performed at 264, 280, 292, and 305 K, using the extended simple point charge model, well suited for reproducing single-particle properties of H_2O. The microscopic dynamics has been probed over a wide range of times and distances. The MD results indicate that a substantial coupling between translational and rotational dynamics exists already at about 1 ps. The decay of the translational dynamic correlations has been phenomenologically analyzed in terms of three exponential components, and the agreement between the parameters thus obtained from experimental and simulation derived datasets is quite satisfactory. Both QENS and MD data can not be described with sufficient accuracy by simple diffusion models over the entire range of examined wave vectors. © *1996 American Institute of Physics.* [S0021-9606(96)50409-2]

I. INTRODUCTION

The dynamic properties of water at the molecular level have been extensively studied in the past years by many different experimental techniques, and a large body of data on microdiffusivity parameters has been accumulated sofar.[1,2] Measurements of viscosity,[3] ultrasound absorption,[4] self-diffusion,[5] dielectric relaxation,[6] NMR,[7] depolarized light scattering,[8–11] and incoherent quasielastic neutron scattering[12–15] have provided information on various relaxation times connected to structures induced by the hydrogen bonds (HB).

During the past two decades, starting from the pioneering molecular dynamics (MD) study of Rahman and Stillinger,[16] the experimental investigations have been increasingly complemented by MD computer simulations in order to get a better insight on the microscopic structure and dynamics of water. Initially much of this work has been focused on the refinement of potential models in order to describe with increasing accuracy those peculiar features of liquid water generally ascribed to HB effects. Subsequently the efforts have been addressed to achieve a full description of the dynamics at the molecular level. Nowadays the increase in computing power, together with the refinements of algorithms and potential models, make it possible to extend the MD simulations up to hundreds of picoseconds, thus probing not only the local short time reorientational dynamics but also the relaxation processes associated with density fluctuations which occur on a much longer time scale. In this context the most appropriate experimental technique to be compared with the MD simulation is the quasielastic scattering of neutrons (QENS). Due to the large incoherent scattering cross section of hydrogen (79.7 barn) with respect to oxygen (<0.002 barn), QENS from H_2O is dominated by the incoherent contribution from protons, and it is therefore sensitive to individual molecular motions. Using time-of-flight and backscattering spectrometers such motions can be followed up to times of the order of hundreds of ps and over distances ranging from the atomic scale up to a few hundred ängströms. In the past 15 years, systematic QENS studies on liquid water, have been carried out on reactor sources using triple axis[13] and time-of-flight spectrometers[12,14,15] with energy resolutions ΔE ranging from about 50 to 500 μeV (half-width at half-maximum, HWHM). In these experiments the diffusional broadening $\Delta\Gamma$ of the elastic peak was analyzed with a limited accuracy, especially in the supercooled regime (0 to -20 °C) which is of particular interest because of the marked anomalies in the thermodynamic and transport properties.[17] Indeed, in this region the broadening $\Delta\Gamma$ turned out to be only a fraction of the instrumental resolution ΔE. The above experiments were however able to clearly identify some general features of the QENS profiles in the 0 to 1 meV region. The spectra showed the presence of two distinct components with substantially different broadenings. The narrow one was attributed to the translational diffusion of water molecules, i.e., to their center-of-mass (CM) dynamics, while the broader one was assigned to the reorientational dynamics around the CM. This interpretation was based on the assumption of a decoupling of the translational, rotational, and vibrational motions. In this case the self-part of the intermediate scattering function can be written as[18]

[a)]Previous address: Istituto di Elettronica Quantistica, C.N.R., Via Panciatichi, 56/30, I-50127 Firenze, Italy.

$$F_s(Q,t)=\exp\left[-Q^2\,\frac{\langle u^2\rangle}{3}\right]F_s^T(Q,t)F_s^R(Q,t). \tag{1}$$

In the quasielastic region the vibrations contribute to the scattering intensity only through a Debye–Waller factor (DW), which is given in the quasiharmonic approximation by the first term in Eq. (1). The narrow spectral component assigned to the translational contribution $F_s^T(Q,t)$ was described in terms of a random, spatially isotropic jump diffusion model (RJD).[19] This choice was suggested by the marked bending of the line broadening at high Q values, which is not consistent with the predictions of simple continuous diffusion models (linear increase of the linewidth vs Q^2). In the frame of the RJD model the F_s^T function can be written as

$$F_s^T(Q,t)=\exp[-\Gamma_T(Q)t] \tag{2}$$

and the width $\Gamma_T(Q)$ can be expressed in terms of a translational diffusion coefficient D_T and a residence time between jumps τ_0 in the form

$$\Gamma_T(Q)=\frac{D_TQ^2}{1+D_TQ^2\tau_0}. \tag{3}$$

Although this simplified model has a high Q limit ($\lim_{Q\to\infty}\Gamma_T(Q)=\tau_0^{-1}$) which contrasts the free-particle behavior ($\Gamma_T\propto Q$, as expected at small length scales), it was able to describe reasonably well the QENS data in the Q range 0.25–2 Å^{-1} covered in the above mentioned experiments.

The broader component of the QENS spectrum was attributed to the rotational dynamics of H_2O molecules, and it was analyzed in terms of the classical Sears expansion describing a continuous isotropic rotational diffusion[20]

$$F_s^R(Q,t)=\sum_l\,(2l+1)j_l^2(Qa)\exp[-l(l+1)\Gamma_R], \tag{4}$$

where l is an integer, $j_l(Qa)$ indicates the spherical Bessel functions, and a is the radius of rotation. In the explored Q range F_s^R was approximated by the first three terms in Eq. (4).

A comparison between MD simulations and the most accurate QENS data available at that time[15] was carried out some years ago.[21] The picture that emerges indicates some disagreement between QENS and MD results. The MD simulations tend to enforce a description of a fairly continuous diffusive dynamics of water, which is quite evident in the high-Q behavior of the calculated broadening of the quasielastic line which does not exhibit the pronounced high-Q saturation observed in QENS measurements.

We have undertaken a systematic study of water dynamics performing high resolution QENS experiments[22] and MD simulations with the following objectives:—to obtain a more accurate determination of the diffusivity parameters of supercooled water by using the high resolution backscattering spectrometer IRIS at the high intensity pulsed neutron source ISIS (DRAL, Chilton, U.K.). In the adopted instrument configuration IRIS has an energy resolution (HWHM) of 5–7 μeV, which is almost an order of magnitude better than that available in the previous experiments, and this allowed us to analyze accurately the small line broadenings observed in the supercooled region. Moreover the high Q resolution ($\Delta Q=0.02$–0.04 Å^{-1} in the Q range 0.4 to 1.85 Å^{-1}) made it possible to determine in detail the Q dependence of the linewidths;—to extend the MD analysis up to times of the order of 100 ps in order to match the energy range probed by QENS, exploiting the potentialities of new high speed CPUs and improved codes for computer simulations. The simulations were performed using a CRAY Y-MP computer (CINECA, Bologna, Italy);—to compare quantitatively high resolution QENS data and realistic MD results. This should enable us to analyze critically the approximations assumed in Eqs. (1) to (4) and, on the other hand, to determine how realistic is the adopted potential in mimicking the self properties of water.

In Secs. II to IV the MD simulations are described in detail. Section V contains a concise description of the QENS experiments. The comparison between MD and QENS results is illustrated in Sec. VI. Conclusions and forthcoming work are outlined in Sec. VII.

II. MOLECULAR DYNAMICS SIMULATIONS

A. Computational aspects

In order to compare the high resolutions QENS data with precise MD results the simulations have been performed in the microcanonical (NVE) ensemble, considering a relatively high number ($N=500$) of rigid "H_2O" molecules enclosed in a cubic box of length $L=24.63$ Å with periodic boundary conditions, and they have been extended to rather long times (i.e., $\simeq$200–300 ps). We adopted a simple rigid water model, namely, the extended simple point charge (SPC/E) potential[23] and developed a new algorithm for the integration of the equations of motion, which combines quickness with a good accuracy.[24] In all the simulations the density has been kept equal to 1 g/cm^3.

Among the relatively simple models for water[23,25–28] present in literature, SPC/E has been chosen because of its capability of well reproducing several static and dynamic properties from the melting point up to the critical point.[29] In particular, the SPC/E model seems quite suitable to simulate single-particle dynamical properties, because it gives values of the self-diffusion coefficient well in agreement with experimental data[23] in a wide range of temperatures along the coexistence curve. SPC/E has been derived from a reparameterization of the simple point charge (SPC) potential[27] to account for the dipole polarizability self-energy correction. Both SPC and SPC/E potentials describe a water molecule by three point charges located on the nuclei plus a Lennard-Jones site centered on the oxygen. The SPC/E parameters are given in Table I.

The electrostatic long range intermolecular interactions have been accounted for by a suitable tapered reaction field (RF).[30] This method has been preferred to Ewald summations[31] since, for large samples, it is less time consuming and does not lead to substantial differences in the values of the main thermodynamical quantities.[32,33] A stan-

TABLE I. SPC/E potential parameters from Ref. 23. The Lennard-Jones interaction potential between the two oxygen atoms is expressed as $V=-(A/r)^6+(B/r)^{12}$. The charges q_H and q_O are located on the corresponding nuclei.

d_{OH} (nm)	$\hat{HOH}$	A (kJ/mol)$^{1/6}$	B (kJ/mol)$^{1/12}$	q_H (e)	q_O (e)
1	109.47°	0.37122	0.3428	0.4238	−0.8476

dard leapfrog algorithm has been adopted for the translational motion, and an improved quaternion integration scheme[24,34] has been used for the rotational motion. In spite of the relatively large time step, $\Delta t=1.5$ fs, the new integration algorithm, together with the tapered RF, leads to an extremely low residual drift of the internal energy: less than 0.002 (kJ mol^{-1})/ps.

After equilibration, we have performed four distinct MD runs at about 264, 280, 292, and 305 K, and the configurations have been stored every 5 time steps, i.e., each 7.5 fs, for successive analysis. The duration t_d of each run is reported in Table II together with the mean temperature T, mean pressure P, total energy U and mean translational self-diffusion coefficient D_T.

B. Evaluation of intermediate scattering functions

As already mentioned, due to the high incoherent scattering cross section of protons, the dynamic structure factor measured by QENS practically coincides with the Fourier-transform of the intermediate self-scattering function $F_s(\mathbf{Q},t)$[35] for the hydrogens

$$F_s(\mathbf{Q},t)=\langle e^{-i\mathbf{Q}\cdot[\mathbf{r}(0)-\mathbf{r}(t)]}\rangle, \tag{5}$$

where $\langle\cdots\rangle$ stands for ensemble average and $\mathbf{r}(t)$ represents the coordinate at time t of a particular hydrogen atom located in $\mathbf{r}(0)$ at time $t=0$. Computationally the average is taken over all the hydrogens of the sample and over each couple of the stored configurations separated by a time t.

In order to examine the coupling between translational and rotational dynamics we have also calculated the intermediate self-scattering function for the motion of the centers of mass, $F_s^{CM}(\mathbf{Q},t)$, and for the reorientational motion (i.e., the hydrogen motions with respect to the CM) $F_s^R(\mathbf{Q},t)$. The expression for F_s^{CM} and F_s^R can be derived by writing (in a fixed reference frame) the position $\mathbf{r}$ of an hydrogen atom pertaining to a given water molecule as

$$\mathbf{r}=\mathbf{r}_{CM}+\mathbf{d},$$

where $\mathbf{d}$ is the position of the hydrogen with respect to the center of mass, $\mathbf{r}_{CM}$. We can then write

$$F_s^T(\mathbf{Q},t)\equiv F_s^{CM}(\mathbf{Q},t)=\langle^{-i\mathbf{Q}\cdot[\mathbf{r}_{CM}(0)-\mathbf{r}_{CM}(t)]}\rangle \tag{6}$$

and

$$F_s^T(\mathbf{Q},t)=\langle e^{-i\mathbf{Q}\cdot[\mathbf{d}(0)-\mathbf{d}(t)]}\rangle. \tag{7}$$

Moreover, in an isotropic fluid all the above intermediate scattering functions must be independent of the direction of $\mathbf{Q}$, and we can therefore improve the statistics by averaging over vectors pointing to different directions, but having the same modulus Q.

For comparison, the three intermediate scattering functions F_s, F_s^{CM}, and F_s^R at 264 K and $Q=1.02$ Å^{-1}, are reported in Fig. 1(a), and their short time behavior ($0\leqslant t\leqslant 0.3$ ps) is shown in more detail in Fig. 1(b). Both F_s^R and F_s reveal an initial very rapid decay, on a time scale of about 0.05 ps; in contrast F_s^{CM} does not show such fast decay. Above 0.05 ps two additional time scales are apparent in F_s and F_s^{CM} as one can see in Fig. 1(a). Above 10–15 ps the differences between F_s^{CM} and F_s tend to vanish and they both approach zero for $t\to\infty$; on the contrary F_s^R has a nonzero horizontal asymptote.

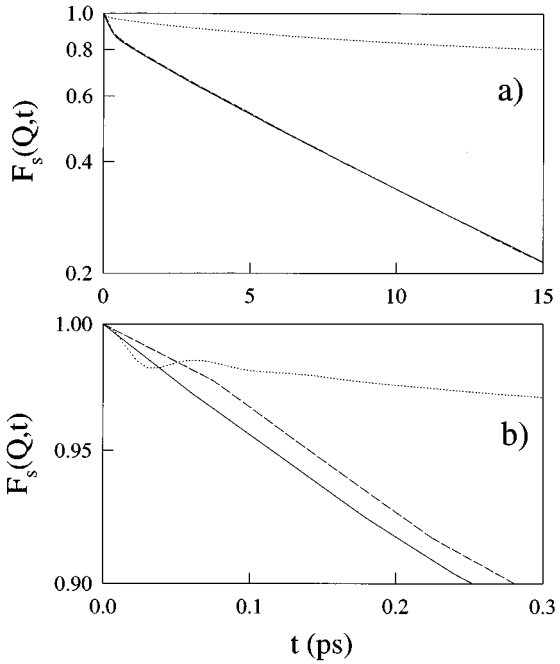

FIG. 1. (a) Total, center-of-mass, and rotational intermediate self-scattering functions at $T=264$ K and $Q=1.02$ Å^{-1}: $F_s(Q,t)$ (solid line), $F_s^{CM}(Q,t)$ (dashed line), and $F_s^R(Q,t)$ (dotted line); (b) Same as in (a) but with a limited time interval ($t\leqslant 0.3$ ps). The initial very rapid decay ($t<0.05$ ps) present in both F_s and F_s^R, and absent in F_s^{CM} is visible.

TABLE II. Thermodynamic data and diffusion coefficients for the MD runs. T denotes the average temperature, t_d the duration of each run, U the total energy, P the average pressure. D_T^{MD} indicates the translational diffusion coefficient obtained from the MD data. D_T and D_T^{QENS} have been derived from tacer diffusion (Ref. 5) and recent neutron scattering data (Ref. 44), respectively.

T (K)	t_d (ps)	U (kJ/mol)	P (MPa)	D_T^{MD} (10^{-5} cm^2/s)	D_T (10^{-5} cm^2/s)	D_T^{QENS} (10^{-5} cm^2/s)
264	315	−42.5	−23.6	1.04	0.75	0.9(5)
280	210	−41.0	−13.5	1.60	1.42	1.5
292	158	−39.9	−6.6	2.(5)	2.25	2.3
305	45	−38.6	5.1	3.(5)	3.12	

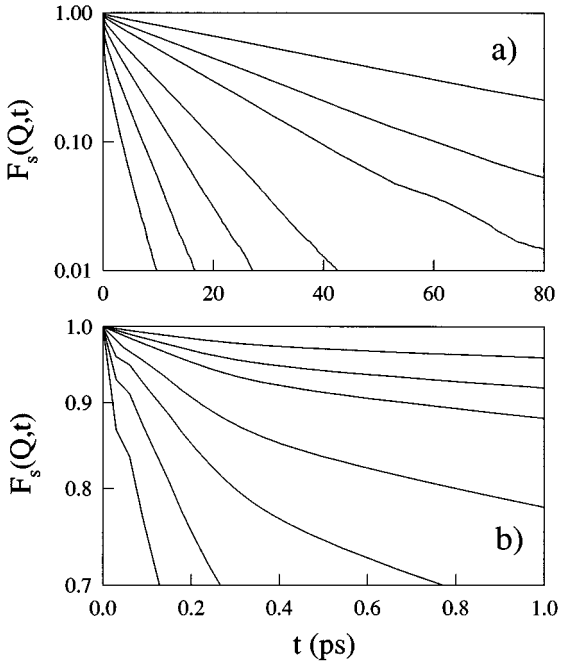

FIG. 2. (a) Total intermediate scattering functions $F_s(Q,t)$ at $T=264$ K and at different Q values: 0.44, 0.62, 0.77, 1.08, 1.40, 1.86, 2.60 Å^{-1} (top to bottom); (b) same as in (a) but with a limited time interval ($t\leqslant 1$ ps).

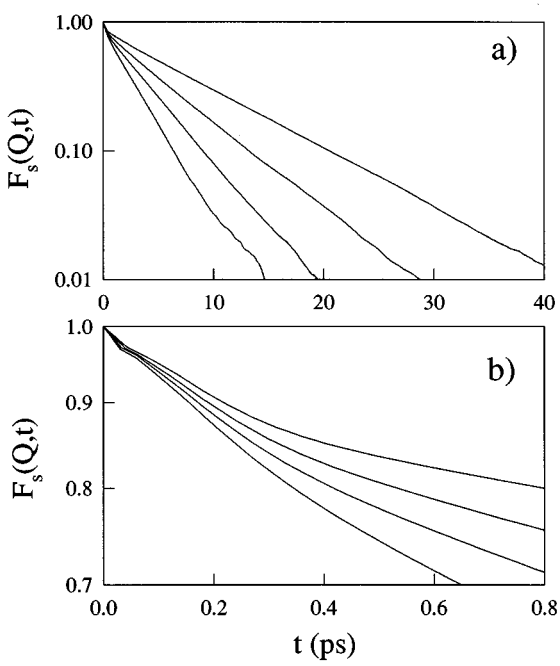

FIG. 3. (a) Total intermediate scattering functions $F_s(Q,t)$ at $Q=1.08$ Å^{-1} and at different temperatures: $T=264$, 280, 292, and 305 K (top to bottom); (b) same as in (a) but with a limited time interval ($t\leqslant 0.8$ ps).

III. DISCUSSIONS OF MD RESULTS

The initial very rapid decay-rates present in F_s and F_s^R are rather similar in the investigated temperature and Q range. As already noticed such a feature is absent in the time behavior of F_s^{CM}. It is therefore natural to ascribe it to the fast reorientational, or rather librational, motions of the hydrogens around the CM.[36,37] In the following analysis of the F_s we will neglect this very rapid decay which takes place in a time interval of only few time steps of our simulations.

As mentioned before, above 0.05 ps a single decay time is generally not sufficient to represent the behavior of the $F_s(Q,t)$ functions in the full investigated time range. Indeed in Figs. 2 and 3, it is possible to recognize easily two main distinct decays, hereafter called fast and slow components. If the F_s are analyzed in term of a superposition of exponential functions, it turn out that at 292 K two exponentials, corresponding to the two above components, are sufficient for a reasonably accurate description. On the other hand, at the lower temperatures (280 and 264 K) a third exponential (characterized by a decay rate intermediate between the previous two) is needed to reproduce the behavior of the F_s at intermediate Q values ($1<Q<2$ Å^{-1}). We have therefore adopted the following empirical expression to describe the time decay of the F_s functions:

$$F_s(Q,t)=A_1(Q)e^{-\Gamma_1(Q)t}+A_2(Q)e^{-\Gamma_2(Q)t}+A_3(Q)e^{-\Gamma_3(Q)t}. \tag{8}$$

The first exponential describes the fast component, the second one describes the slow component and the third one the ''intermediate'' component which is needed to reproduce with sufficient accuracy the crossover region between the fast and slow decays. In Fig. 4 a fit of $F_s(Q,t)$ to Eq. (8) is shown; the Q value (1.8 Å^{-1}) has been chosen such that all the components are clearly visible. The same data fitted with only two exponentials are shown in Fig. 5. The residuals of

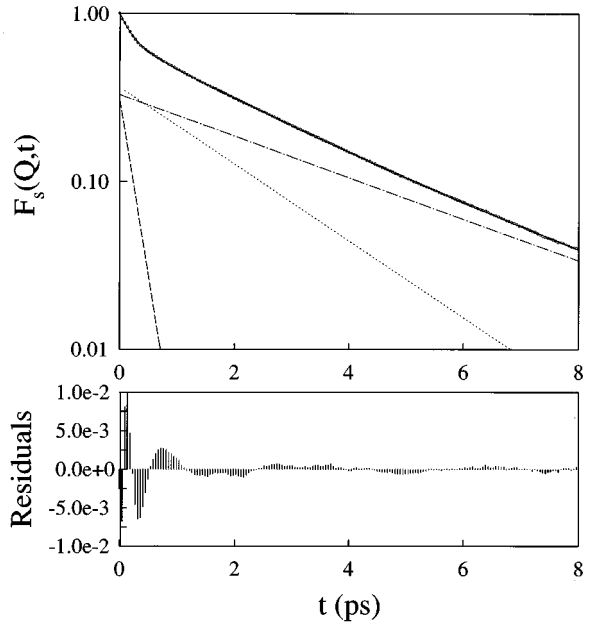

FIG. 4. Fitting of $F_s(Q,t)$ ($Q=1.8$ Å^{-1}, $T=264$ K) to Eq. (8). In this case the three exponential components (fast: dashed line; intermediate: dotted line; slow: dot–dashed line) have similar amplitudes A_i. The residuals of the fitting are also shown.

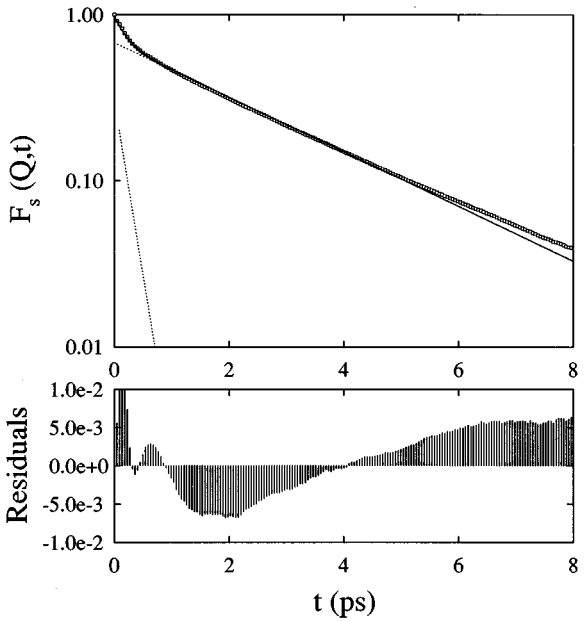

FIG. 5. Fitting of $F_s(Q,t)$ ($Q=1.8$ Å^{-1}, $T=264$ K) to the sum of two independent exponentials. The residuals of the fitting are also shown.

the fitting shown in both figures evidence the improvement obtained by adding the third intermediate component. This improvement can be estimated quantitatively by comparing the χ^2 values obtained from the two above analyses. In Fig. 6 the ratio of the χ^2 values obtained by fitting the above data with two and three exponentials, respectively, is shown vs Q for 264 and 292 K. At the lowest temperature this ratio increases by almost an order of magnitude in the $1<Q<2$ Å^{-1} region, while at 292 K the ratio is almost constant and close

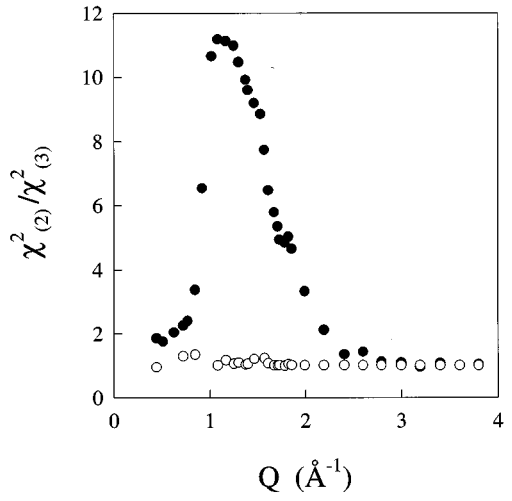

FIG. 6. Dependence upon Q of ratio of the χ^2 values obtained by fitting the $F_s(Q,t)$ functions with two and three independent components, respectively. The data at 264 K (full circles) and at 292 K (empty circles) are reported. The χ^2 ratio at 280 K is very close to the one at 264 K.

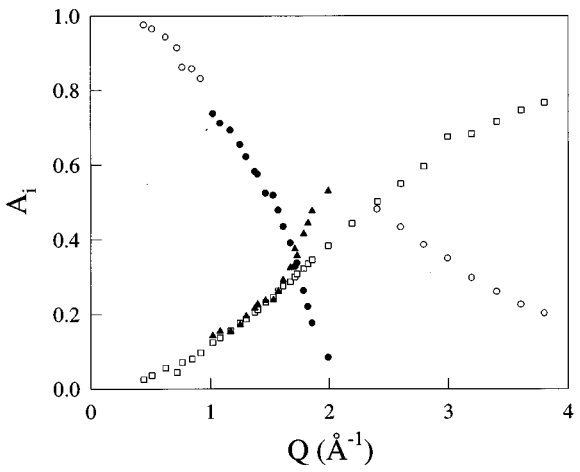

FIG. 7. Amplitudes A_i of the three exponential components at 264 K derived from the fit of the MD intermediate scattering functions $F_s(Q,t)$: A_1 (empty squares), A_2 (circles), A_3 (full triangles). The amplitude A_3 is reported only in the Q region where it is appreciably different from zero; in this region A_2 is indicated with full circles.

to unity at all Q values. All fittings have been performed using a standard least-squares minimization routine.

At small Q values, the amplitude A_1 of the fast component is much smaller than the amplitude of the slow one A_2. The dependence of A_1, A_2, and A_3 upon Q is shown in Fig. 7 for the simulations at 264 K. The behavior of the coefficients A_i at 280 K is quite similar, while at 292 K the addition of the third component (A_3) does not improve the fits significantly, as already anticipated.

In the frequency domain, Eq. (8) corresponds to a representation of the incoherent dynamic structure factor $S_s(Q,\omega)$ [i.e., the time-Fourier transform of $F_s(Q,t)$] in terms of a sum of three Lorentzian components with half-width at half-maximum (HWHM) equal to the Γ_i. In the following the values of the Γ parameters are reported as HWHM in energy units (μeV) to allow a direct comparison with the line broadenings of the QENS spectra. In Figs. 8 and 9 the Q dependence of Γ_1, Γ_2, and Γ_3 is shown for different temperatures. Γ_1, which is clearly visible only above $Q\simeq 1$ Å^{-1}, has a noticeably linear Q dependence at high Q values (Fig. 8). Indeed, the scattering law in the free particle limit has a Gaussian shape, and its width is given by[38]

$$\Gamma(Q)\approx Q\sqrt{\frac{k_B T 2\ln 2}{m}} \tag{9}$$

this behavior is also expected for a particle moving in a liquid, when the probed length scale is small with respect to the interatomic distances. In the present case our highest Q values are much too low to reveal the free particle limit, however, the quasilinear dependence of Γ_1 at high Q in Fig. 8 can be considered as an indication that the fast decay can be associated to the quasifree motion of a water molecule within the cage formed by its neighboring molecules.

The Q dependence of Γ_2, as shown in Fig. 9, is linear vs Q^2 at low Q, then it bends over but never reaches a total

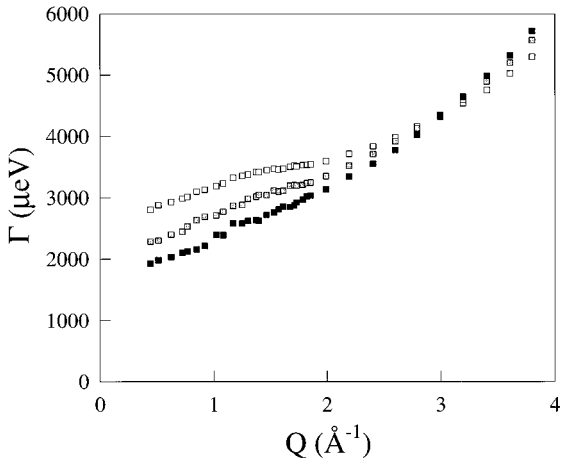

FIG. 8. Decay constant Γ_1 vs Q from the fit of MD simulations at different temperatures: 292 K (full squares), 280 K (gray squares) and 264 K (empty squares).

flattening up to the highest Q investigated, this confirms the results of a previous MD study.[21] The obtained Q dependence of the amplitudes A_i and of the widths Γ_i cannot be explained by simple diffusion models, neither of jump, nor of continuous type. The constant breaking and reforming of the HB network suggested by the MD simulations[39] seems to favor a description in terms of a complex continuous-type diffusion.

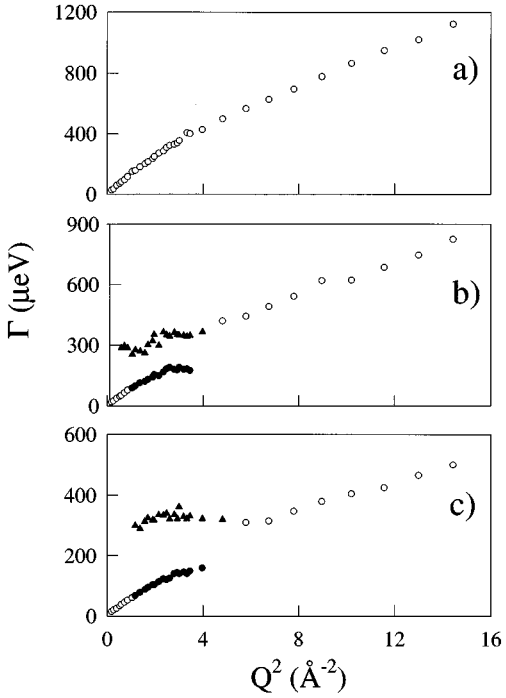

FIG. 9. Decay constants Γ_2 (open circles) and Γ_3 (full triangles) vs Q^2 from MD results, for different temperatures: (a) 292 K, (b) 280 K, (c) 264 K. Γ_3 is reported only in the Q region where the amplitude A_3 is appreciably different from zero; in this region Γ_2 is indicated with full circles.

The overall behavior of $F_s^{\mathrm{CM}}(Q,t)$ is very similar to that of $F_s(Q,t)$. Their fit still requires two main exponential components (the above mentioned fast and slow processes). At 280 and 264 K, a third exponential improves substantially the fit between $Q=1$ and 2 Å^{-1}. The values of the parameters A_i and Γ_i derived from the fit are sometimes slightly different from those obtained from $F_s(Q,t)$; such small differences have not been considered to be significant in our analysis. The presence in F_s^{CM} of the same features observed in F_s, namely the presence of fast, slow, and intermediate components, indicates that they are all related to the translational dynamics. Roughly speaking the fast one can be related to the free particle dynamics within the nearest neighbor cage, while the slow and intermediate ones may be related to more complex mechanisms of H_2O cluster relaxations. It is worth noticing that even in the case of simple liquids, such as liquid argon, $F_s(Q,t)$ has a complex t and Q dependence[38] not fully describable as the superposition of two (or three) exponentials. An interpretation of the $F_s^{\mathrm{CM}}(Q,t)$ for water in terms of a memory function approach will be reported in a forthcoming paper.

The diffusion coefficient D_T has been evaluated from the slope of the mean square displacement (MSD) and from the area below the velocity autocorrelation functions (VACF) obtaining results well in agreement with each other. In Table II we report only the results relative to the MSD which are less affected by statistical uncertainties. For the sake of comparison, in Table II some experimental values of D_T are also reported. At each temperature, the agreement among the different data is satisfactory and confirms that the adopted potential model can effectively reproduce the microscopic translational dynamics of liquid water.

As shown in Fig. 1(b), the rotational functions $F_s^R(Q,t)$ are characterized by a very rapid decay at short times ($t<0.05$ ps) followed by a damped oscillation probably attributable to a partially librational nature of the rotational relaxation and, at $t\geqslant 1$ ps, by a much slower relaxation to a nonzero asymptotic value. The short time region including the damped oscillation has not been explored in great detail, indeed it is covered by a small number of time steps in our simulations. The overall time behavior of the F_s^R functions has been analyzed in terms of two exponential decays with widths Γ_1^R and Γ_2^R corresponding to the very fast and slow relaxations, respectively, plus a constant term (B) giving the $t\rightarrow\infty$ asymptote

$$F_s^R(Q,t)=A_1^R(Q)e^{-\Gamma_1^R(Q)t}+A_2^R(Q)e^{-\Gamma_2^R(Q)t}+B. \qquad (10)$$

This model was found to be adequate at small and intermediate Q values, only at the highest Q investigated the decay could not be accurately described by Eq. (10).

From the fit of the $F_s^R(Q,t)$ functions to Eq. (10), we find that Γ_1^R is substantially Q and temperature independent, with an average value of about 20 meV (HWHM). The width of the slower relaxation, Γ_2^R, is Q independent as well, but shows a moderate variation with temperature; its values range from 70 μeV at 264 K, to 85 and 120 μeV at 280 and 292 K, respectively. The amplitudes A_i^R, on the other hand,

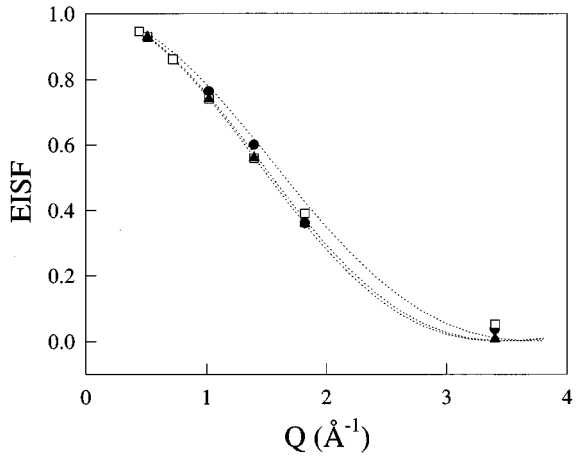

FIG. 10. Elastic incoherent structure factors EISF derived from the MD rotational intermediate scattering functions F_s^R at different temperatures: 292 K (full circles), 280 K (open squares), and 264 K (full triangles). The fittings to the expression in Eq. (12) are shown (dotted lines).

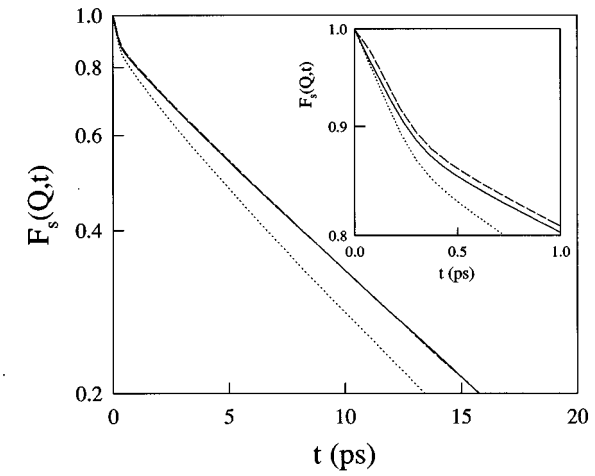

FIG. 11. (a) Time dependence of the intermediate scattering functions at $T=280$ K and $Q=1.02$ Å^{-1}; $F_s(Q,t)$ (solid line), $F_s^{\mathrm{CM}}(Q,t)$ (dashed line) and $F_s^P(Q,t) = F_s^{\mathrm{CM}}(Q,t) \cdot F_s^R(Q,t)$ (dotted line). The time region $t \leqslant 1$ ps is shown in the inset.

are almost temperature independent, but they both markedly depend on Q. The ratio A_2^R/A_1^R decreases continuously from 8 at $Q=0.42$ Å^{-1} down to 2.7 at $Q=3.4$ Å^{-1}.

The nonzero asymptotic value ($t\rightarrow\infty$) is due to the confined motion of the hydrogens when observed from their CM reference frame. In this frame they are limited to move on the surface of a sphere of radius $d=|\mathbf{d}|$ and, as a consequence, $F_s^R(Q,t\rightarrow\infty)$ must have a nonzero value.[40] The spatial extension of these motions can be evaluated through the so called ''elastic incoherent structure factor'' (EISF) defined as

$$\mathrm{EISF}=\frac{F_s(Q,t\rightarrow\infty)}{F_s(Q,t=0)}. \tag{11}$$

For a particle diffusing isotropically on a sphere of radius d, it can be shown[40] that

$$\frac{F_s^R(Q,t\rightarrow\infty)}{F_s^R(Q,t=0)}=[j_0(Qd)]^2=\left[\frac{\sin(Qd)}{Qd}\right]^2. \tag{12}$$

The behavior of the EISF, as obtained from the simulations, is reported in Fig. 10. By fitting its Q dependence to Eq. (12) we have obtained for the radius d: 0.84, 0.90, and 0.91 Å at 264, 280, and 292 K, respectively. The fitted radius increases with temperature as expected, but remains always lower than the H-to-CM distance of the SPC/E model (0.964 Å), indicating that the rotational motion is highly hindered even at room temperature.

IV. ANALYSIS OF THE DECOUPLING BETWEEN TRANSLATIONAL AND ROTATIONAL MOTIONS

The experimental data on water diffusivity obtained up to now by radiation scattering techniques as QENS and light scattering have been usually analysed under the assumption of the decoupling of translational and rotational dynamics [Eq. (1)]. This hypothesis is questionable for molecular liquids, especially when H bonds play a relevant role, like in water. Indeed the assumption made in Eq. (1) has been motivated essentially because it leads to relatively simple analytical expressions for the scattering law, rather than being based on a realistic description of the dynamics at a molecular level. Neglecting the DW factor in Eq. (1), one can express $F_s(Q,t)$ as the product

$$F_s(Q,t)\equiv F_s^P(Q,t)=F_s^{\mathrm{CM}}(Q,t)F_s^R(Q,t). \tag{13}$$

On the other hand, if the rotational and translational motions were strongly coupled, in the long time limit one should have

$$F_s(Q,t)\approx F_s^{\mathrm{CM}}(Q,t). \tag{14}$$

MD simulations provide an effective way for testing the validity of the decoupling approximation. The intermediate scattering functions F_s^P and F_s^{CM} can be evaluated separately through Eqs. (6) and (7) and compared to F_s as obtained from Eq. (5). Figure 11 shows F_s, F_s^P and F_s^{CM} at 280 K and $Q=1.02$ Å^{-1}. It can be seen that at times larger than about 10 ps $F_s(Q,t)$ stays much closer to $F_s^{\mathrm{CM}}(Q,t)$ than to the product $F_s^P(Q,t)$.

In order to quantify the extent of the rotational-translational coupling, we introduce a ''coupling'' indicator defined as

$$I_C(Q,t)\equiv\frac{F_s(Q,t)-F_s^P(Q,t)}{F_s^{\mathrm{CM}}(Q,t)-F_s^P(Q,t)} \tag{15}$$

which ranges from 0 (decoupling) to 1 (full coupling). In Fig. 12 the time dependence of I_C is shown for three different values of Q and temperature. I_C shows an initial fast raise up to $t\sim0.3$ ps, and a further slower increase at longer times. The value of I_C at 0.3 ps decreases with raising temperature, and increases with Q. It is also worth noticing that only in the low-Q range ($Q\leqslant1$ Å^{-1}), and at high temperatures a full coupling is not reached even at relatively long times. Above $Q\sim1$ Å^{-1} a substantial coupling is always achieved already at $t\sim1$ ps.

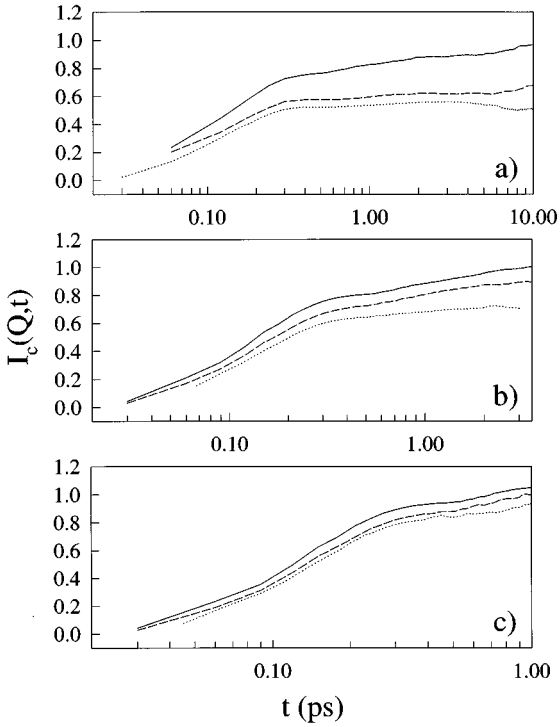

FIG. 12. Coupling indicators I_c at various wave vectors and temperatures. (a) 1.02 $Å^{-1}$, (b) 1.82 $Å^{-1}$, (c) 3.40 $Å^{-1}$. The curves in each figure refer to 264, 280, 292 K, respectively (top to bottom).

V. QUASIELASTIC NEUTRON SCATTERING

We have performed accurate QENS measurements on supercooled H_2O using the IRIS backscattering spectrometer at the ISIS pulsed neutron facility (DRAL, Chilton, U.K.). The experimental details including data corrections and analysis have already been described elsewhere.[22] Here, we will recall the main results of these experiments which are relevant for a comparison between QENS and MD simulations.

IRIS is a backscattering spectrometer[41] viewing a 25 K liquid-hydrogen cold source. In the adopted instrument configuration we used the 002 reflection from pyrolytic graphite (PG) analyzer crystals, and the 006 reflection from mica analyzers. They enabled us to span a Q range from 0.4 to 1.85 $Å^{-1}$ (with a resolution $\Delta Q \simeq 0.02$–0.04 $Å^{-1}$), and provided an energy window from -0.25 to $+1.2$ meV with resolutions (HWHM) 7 μeV (graphite) and 5.5 μeV (mica). The space and time domains covered range from about 3 to 15 Å and from 0.5 to 50 ps. These data have been already analyzed[22,42] in terms of the same line-broadening model used in the earlier QENS experiments on supercooled water;[15] such model has been described in Sec. I. On the basis of the MD results which indicate a substantial coupling between translational and rotational motions in the energy range explored with IRIS, we have now analyzed the line shapes in terms of the phenomenological model adopted in Eq. (8). The MD simulations give for the fast component in Eq. (8) a width ranging from 2 to 6 meV (Fig. 8), i.e., much larger than the total energy window accessible with IRIS. Therefore, in the QENS analysis, this contribution was taken into account by a Lorentzian component whose width was constrained to be equal to the corresponding one of the MD simulation. In the measured energy range this component could be equally well represented by a flat background level. Figure 13 shows the decomposition of a typical line shape into a flat background, and two Lorentzian components corresponding to the slow and intermediate contributions in Eq. (8). The background includes the fast component and an instrumental contribution. The widths Γ_2 and Γ_3 obtained from the above fitting are shown as a function of Q^2 in Fig. 14.

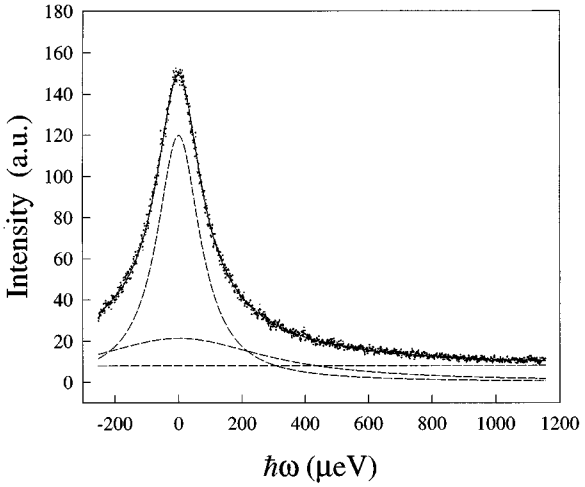

FIG. 13. Example of the decomposition of a QENS spectrum ($Q=1.41$ $Å^{-1}$ and $T=264$ K) into three quasielastic rototranslational components; Lorentzian line shapes are assumed. The third component, as explained in the text, is backgroundlike in the investigated energy range.

At high temperatures ($T \geqslant 280$ K) and high Q values ($Q \geqslant 1.5$ $Å^{-1}$) only one Lorentzian is needed. The Q dependence of Γ_2 is linear vs Q^2 at low Q, then it bends over and tends to flatten, but, up to the highest Q investigated, it does

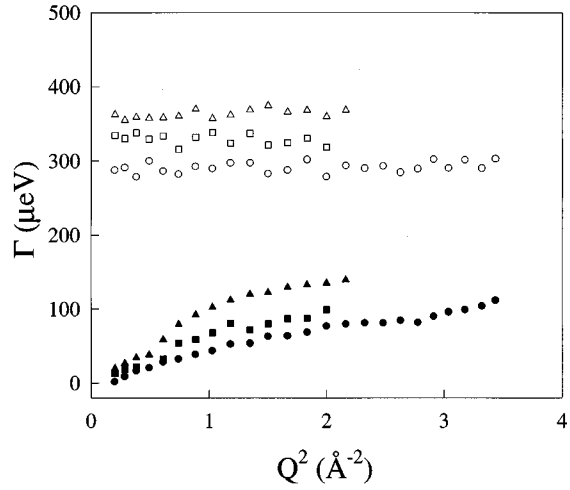

FIG. 14. Quasielastic broadenings Γ_2 (full symbols) and Γ_3 (open symbols) vs Q^2 derived from the fitting of the QENS data. The curves refer to 264 K (circles), 278 K (squares), and 292 K (triangles).

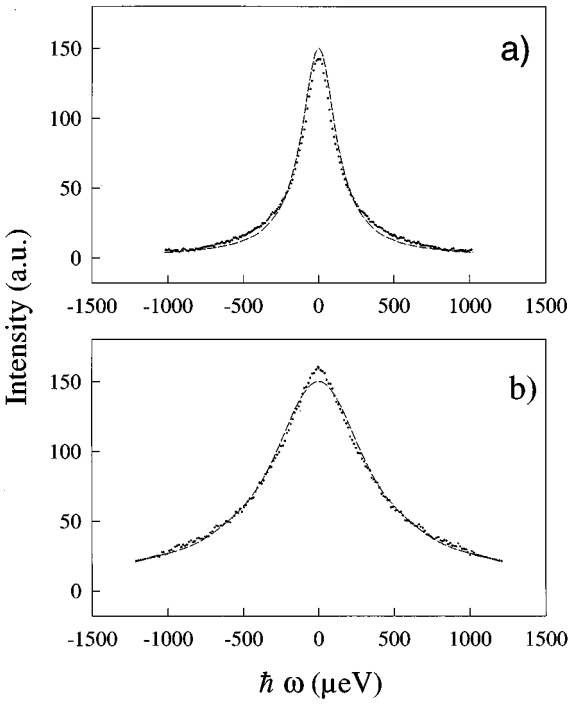

FIG. 15. Comparison of QENS and MD dynamic scattering functions $S_s(Q,\omega)$ at $T=264$ K and $Q=1.02$ (a), 1.80 (b) Å^{-1}.

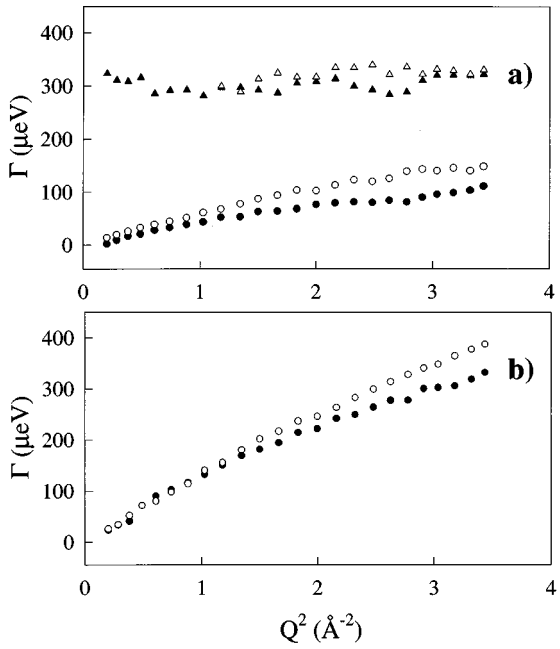

FIG. 16. Comparison of the Q dependence of the linewidths Γ_i obtained from QENS experiments (full symbols) and MD simulations (open symbols). The data are reported for two temperatures: 264 K (a), and 292 K (b), and refer to Γ_2 (circles) and Γ_3 (triangles).

not reach a complete plateau. On the contrary Γ_3 is almost constant in the investigated Q range. Both the linewidths Γ_2 and Γ_3 increase with temperature.

VI. COMPARISON BETWEEN THE QENS AND MD DYNAMIC STRUCTURE FACTORS

The noise level present in the F_s functions from MD simulations in much lower than that of the analogous functions obtained by Fourier inversion of the experimental spectra. For this reason, in order to compare the QENS results with the MD simulations, we decided to Fourier transform the latter, and perform the comparison in the ω domain. For this purpose standard Hanning function has been used to apodize the finite time signal,[43] and the F_s have been evaluated from our MD runs up to times long enough to allow an almost complete decay of the correlations. Moreover to check the accuracy of the Fourier transformations we have verified that the analysis in t and ω domains give consistent values of the parameters A_i and Γ_i.

Figure 15 shows a comparison of two line shapes obtained from the MD data and from the QENS experiment for two different Q values. The areas of the experimental curves have been normalized to those of the MD after subtraction of the experimental background. The agreement between experimental and MD data is reasonable both at low and at high Q values. The linewidth parameters Γ_2 and Γ_3 obtained by fitting the QENS and MD data are compared in Fig. 16. At the lowest investigated temperature (264 K) the experimental Γ_2 is always lower than the one from MD, and the difference among them increases with Q reaching a maximum value of about about 30% [Fig.16(a)]. As concerns Γ_3, we note that for a satisfactory fit of the experimental data this component is required at all Q values at 264 K, and up to at least 1.5 Å^{-1} at 280 and 292 K. On the other hand, in the MD fits Γ_3 is needed only at $1 \leqslant Q \leqslant 2$ Å^{-1} at 264 and 280 K, while at 292 K it is never required. At 264 and 280 K, and in the Q range where Γ_3 has to be introduced in the fit of both simulated and experimental data, their respective values differ only by about 10% [Fig. 16(a)]. On the other hand, for a consistent comparison between QENS and MD data at 292 K, their respective fits with only one Lorentzian component have been compared [Fig. 16(b)]; it must, however, be kept in mind that the addition of a second component substantially improves the fit of QENS data. The QENS and MD widths agree well up to about 1.2 Å^{-1}, at higher Q values the MD width increases faster, and the maximum difference between the two is about 15% at 1.85 Å^{-1}.

As concerns the amplitudes A_i, a difference exists: at any given Q and temperature the third intermediate component is consistently more intense in the experimental data than in the simulated ones. It turns out that at 280 K $A_2^{\mathrm{QENS}}/A_2^{\mathrm{MD}}$ has a Q averaged value of about 0.7, while $A_3^{\mathrm{QENS}}/A_3^{\mathrm{MD}}$ is about 4.

VII. CONCLUSIONS

We have performed a detailed comparative analysis of MD simulations and high energy resolution QENS experiments in supercooled H_2O with the aim of improving similar previous studies whose conclusions were rather qualitative.[21] The SPC/E model proved to be an appropriate ''simple'' ef-

fective potential for reproducing the single particle water dynamics at all investigated time and length scales.

The use of a second generation backscattering neutron spectrometer has improved by almost an order of magnitude the resolution of the measurements with respect to previous QENS experiments on supercooled water,[15] this is particularly important to investigate the dynamics in the supercooled region where the diffusional broadenings are considerably smaller than the ones at room temperature.

The comparison has shown that the time decay of the translational dynamic correlations can be phenomenologically described in terms of at least three distinct exponential components. The agreement between amplitudes and width parameters of these components obtained from QENS and MD data is quite reasonable, being always $\leqslant$30%. However, in the QENS spectra the role of the third intermediate component is consistently more relevant than in the MD simulations. This is not totally surprising if we consider that this component essentially describes the deviations from the simple two exponential regimes [fast and slow components in $F_s(Q,t)$], and thus reflects details in the complex translational dynamics of water molecules, which the MD simulation is not able to reproduce accurately, owing to the approximations implied in the adopted potential and possibly to the relative small number of molecules used in the simulation.

Neither the QENS, nor the MD data can be convincingly described by simple diffusion models. The present results open the way to more refined theoretical analysis of the self-dynamics of the density fluctuations in liquid water, in a way similar to the comprehensive description already depicted in simple liquids.[38]

ACKNOWLEDGMENTS

We thank U. Balucani, F. Cavatorta, H. D. Middendorf, G. Ruocco, and R. Vallauri for useful discussions. We acknowledge the *Centro di Calcolo Interuniversitario dell'Italia Nord-Orientale* (CINECA) which made available free of charge part of the CRAY time utilized. Financial support by the *Istituto Nazionale di Fisica della Materia* (INFM), and by the *Consiglio Nazionale delle Ricerche* (CNR) is gratefully acknowledged. One of us (A.T.) gratefully acknowledges also the E.E.C. for the research fellowship No. ERBCHBICT941569.

[1] D. Eisenberg and W. Kauzmann, *The Structure and Properties of Water* (Oxford University, London, 1969).
[2] *Water: A Comprehensive Treatise*, edited by F. Franks, Vol. 1–7 (Plenum, New York, 1972–1982).
[3] J. Hallet, Proc. Phys. Soc. London **82**, 1046 (1963).
[4] G. D' Arrigo and A. Paparelli, J. Chem. Phys. **88**, 7687 (1988).
[5] H. R. Pruppacher, J. Chem. Phys. **56**, 101 (1972); R. Mills, *ibid.* **77**, 685 (1973).
[6] G. Salvetti, in *Hydrogen-bonded Liquids*, edited by J. C. Dore and J. Teixeira (Dordrecht, Kluwer, 1991), p. 369.
[7] K. T. Gillen, D. C. Douglas, and J. M. R. Hoch, J. Chem. Phys. **57**, 5117 (1972); R. J. Speedy, F. X. Prielmeier, T. Vardag, E. W. Lang, and H. D. Ludemann, Mol. Phys. **66**, 577 (1989).
[8] F. Aliotta, C. Vasi, G. Maisano, D. Majolino, F. Mallamace, and P. Migliardo, J. Chem. Phys. **84**, 4731 (1986).
[9] A. De Santis, R. Frattini, M. Sampoli, V. Mazzacurati, M. Nardone, M. A. Ricci, and G. Ruocco, Mol. Phys. **61**, 1199 (1987); M. A. Ricci, G. Ruocco, and M. Sampoli, Mol. Phys. **67**, 19 (1989).
[10] V. Mazzacurati, M. A. Ricci, G. Ruocco, and M. Sampoli, Chem. Phys. Lett. **159**, 383 (1989); V. Mazzacurati, A. Nucara, M. A. Ricci, G. Ruocco, and G. Signorelli, J. Chem. Phys. **93**, 7767 (1990).
[11] Y. Marechal, in *Hydrogen-bonded Liquids*, edited by J. C. Dore and J. Teixeira (Dordrecht, Kluwer, 1991), p. 237.
[12] J. D. Irish, W. G. Graham, and P. A. Egelstaff, Can. J. Phys. **56**, 373 (1978).
[13] S. H. Chen, J. Teixeira, and R. Nicklow, Phys. Rev. A **26**, 3477 (1982).
[14] M.-C. Bellissent-Funel, R. Kahn, A. J. Dianoux, M. P. Fontana, G. Maisano, P. Migliardo, and F. Wanderlingh, Phys. Rev. A **31**, 1913. (1985).
[15] J. Teixeira, M.-C. Bellissent-Funel, S. H. Chen, and A. J. Dianoux, Phys. Rev. A **31**, 1913 (1985).
[16] A. Rahman and F. H. Stillinger, J. Chem. Phys. **55**, 3336 (1971).
[17] C. A. Angell, in *Water, a Comprehensive Treatise*, edited by F. Franks (Plenum, New York, 1982), Vol. 7.
[18] M. Bée, *Quasielastic Neutron Scattering* (Hilger, Bristol, 1988).
[19] P. A. Egelstaff, *An Introduction to the Liquid State* (Academic, London, 1967).
[20] V. F. Sears, Can. J. Phys. **45**, 237 (1967).
[21] J. Ullo, Phys. Rev. A **36**, 816 (1987).
[22] F. Cavatorta, A. Deriu, D. Di Cola, and H. D. Middendorf, J. Phys. Condens. Matter **6**, A113 (1994).
[23] H. J. C. Berendsen, J. R. Grigera, and T. P. Straatsma, J. Phys. Chem. **91**, 6269 (1987).
[24] G. Ruocco and M. Sampoli, Mol. Phys. **82**, 875 (1994).
[25] F. H. Stillinger and A. Rahman, J. Chem. Phys. **60**, 1545 (1974).
[26] O. Matsuoka, E. Clementi, and M. Yoshimine, J. Chem. Phys. **64**, 1351 (1976).
[27] H. J. C. Berendsen, J. P. M. Postma, W. F. van Gunsteren, and H. J. Hermans in *Intermolecular Forces*, edited by B. Pullman (Reidel. Dordrecht, 1981), p. 331.
[28] W. L. Jorgensen, J. Chandrasekhar, J. D. Madura, R. W. Impey, and M. L. Klein, J. Chem. Phys. **79**, 926 (1983).
[29] Y. Guissani and P. Guillot, J. Chem. Phys. **99**, 8221 (1993).
[30] Adams, E. M. Adams, and G. J. Hills, Mol. Phys. **38**, 387 (1989).
[31] M. P. Allen and D. J. Tildesley, *Computer Simulations of Liquids* (Oxford University, London, 1987).
[32] G. Ruocco, M. Sampoli, A. Torcini, and R. Vallauri, J. Chem. Phys. **99**, 8095 (1993).
[33] U. Balucani, G. Ruocco, M. Sampoli, A. Torcini, and R. Vallauri, in *Hydrogen Bond Networks*, edited by M.-C. Bellissent-Funel and J. C. Dore (Kluwer Academic, Dordrecht, 1994), p. 405.
[34] D. Fincham, Mol. Simul. **8**, 165 (1992).
[35] J. P. Boon and S. Yip, *Molecular Hydrodynamics* (McGraw-Hill, New York, 1980).
[36] M. Wojcik and E. Clementi, J. Chem. Phys. **85**, 6085 (1986).
[37] R. Frattini, M. A. Ricci, G. Ruocco, and M. Sampoli J. Chem. Phys. **92**, 2540 (1990).
[38] U. Balucani and M. Zoppi, *Dynamics of the Liquid State* (Clarendon, Oxford, 1994); U. Balucani, A. Torcini, A. Stangl, and C. Morkel, Phys. Scr. **T57**, 13 (1995).
[39] D. Bertolini, M. Cassettari, M. Ferrario, P. Grigolini, G. Salvetti, and A. Tani, J. Chem. Phys. **91**, 1179 (1989); D. Bertolini, P. Grigolini, and A. Tani, *ibid.* **91**, 1191 (1989).
[40] A. J. Dianoux and F. Volino, Mol. Phys. **34**, 1263 (1977).
[41] C. J. Carlile and M. Adams, Physica B **182**, 431 (1992).
[42] D. Di Cola, Ph.D. thesis, University of Parma, 1995.
[43] A. V. Oppenheim and R. W. Schafer, *Discrete-Time Signal Processing* (Prentice Hall, Englewood Cliffs, 1989).
[44] The D_T^{QENS} data have been calculated in Ref. 42 using the RJD model [Eq. (3)]. However, the obtained values are practically independent of the model adopted.